Supplemental Material

Supplemental Methods

Human and Mouse Platelet Isolation. Whole blood from humans or mice was drawn into acid-citrate-dextrose (ACD) and platelets were isolated as previously described (39, 45). Freshly-isolated platelets were resuspended in M199 culture medium for each experiment.

Assessment of human megakaryocyte activation and adhesion. To measure megakaryocyte spreading and adhesion, day 13 $CD34^+$ progenitor cell derived megakaryocytes were placed on immobilized human fibrinogen (100 μg/ml; Calbiochem-Novabiochem Corporation, San Diego, CA) coated glass cover slips and incubated 2-6 hours in the presence or absence of inhibitors (described above), controls (DMSO), or media alone. After indicated time points, cells were fixed with 4% paraformaldehyde for 20 minutes at room temperature followed by permeabilization in 0.1% Triton-X 100 for 5 minutes. Fixed and permeabilized cells were stained with Alexa fluor 488 Phalloidin, Alexa fluor 555 Wheat Germ Agglutinin (WGA), and TO-PRO 3 (Life Technologies, Grand Island, NY). Cells were imaged using an FV300 Olympus IX81 microscope (Melville, NY). Adherent cells were quantified by counting five 20x fields per chamber. All quantifications were done by a blind observer.

To measure activation, $CD34^+$ progenitor cell derived megakaryocytes were isolated as above. Megakaryocytes were treated with thrombin and PAC-1 binding was measured as described previously by us (38). Fibrinogen binding was also determined in megakaryocytes using published methods from our group. (51).

Ex vivo assessment of megakaryocyte numbers in bone marrow and spleen. A rabbit anti-human von-Willebrand factor (vWF) antibody known to cross-react with murine vWF (Dako, Denmark) was used as the primary antibody to immunohistochemically stain megakaryocytes present in the bone marrow or spleen of *Psmc1*$^{fl/wt}$ and *Psmc1*$^{fl/fl}$*;Pf4cre* mice. A biotinylated horse anti-rabbit antibody was used as the secondary antibody, and color development was achieved with DAB substrate following the Vector Elite ABC kit protocols (Vector, Burlingame, CA). Megakaryocytes, identified by vWF staining in conjunction with morphological features, were then quantified using an eyepiece reticle that delineates an area of tissue measuring 250 x 250 μm at 400X (Klarmann Rulings Inc, Litchfield, NH). The megakaryocyte concentration was expressed as number of megakaryocytes in an area of bone marrow or spleen measuring 250 x 250 μm.

Ex vivo assessment of platelet aggregation. Platelet aggregation studies were performed as previously described (8). Briefly, washed platelets were resuspended in HBSS with 0.5% human serum albumin and preincubated with bortezomib or vehicle control for 30 minutes at 37^{o}C. Treated platelets were then stimulated with 0.05 U/ml or 0.2 U/ml thrombin and aggregation was monitored by transmittance (Chronolog) with stirring (600 rpm).

Ex vivo assessment of mouse and human platelet activation. Washed mouse platelets (1 x 10^{6}) were resuspended in M199 media, pretreated for 30 minutes with bortezomib or its vehicle, and then left alone or activated for 15 minutes with varying concentrations of U46619, convulxin, or Par4 in the presence of PE-JonA (Emfret Analytics, Eibelstadt, Germany), an antibody that recognizes the active form of integrin $\alpha_{IIb}\beta_3$. Agonist-induced expression of surface P-selectin expression (Santa Cruz Biotech, Santa Cruz, CA) was also assessed by flow cytometry in separate experiments.

Washed human platelets ($5x10^8$ total) were resuspended in M199 medium containing 100µg/ml of fibrinogen and were pretreated for 30 minutes with bortezomib or its vehicle. Platelets were then stimulated with U46619, ADP, or thrombin for 15 minutes in the presence of PAC-1 (BD Biosciences, Franklin, NJ), an antibody that binds to the active conformation of integrin $\alpha_{IIb}\beta_{3.}$. Platelets were analyzed immediately using a FacScan.

Supplemental Figures and Table Legend

Supplemental Figure 1. *Bortezomib does not directly activate or alter Par4-induced activation in mouse platelets.* Washed mouse platelets were left alone or incubated with increasing concentrations of Par4. After 15 minutes, JonA binding was assessed by flow cytometry. The bars represent the mean±SEM of 3 independent experiments.

Supplemental Figure 2. *Inhibition of the proteasome ex vivo does not alter the function of mouse platelets.* Washed mouse platelets were pretreated with Bort or its Veh and subsequently stimulated with increasing concentrations of U46619 or convulxin as described in the Methods section. After 15 minutes, JonA binding (**A**) or P-selectin surface expression (**B**) was assessed by flow cytometry. The bars represent the mean±SEM of 3 independent experiments.

Supplemental Figure 3. *Inhibition of the proteasome ex vivo does not alter the function of human platelets.* Washed human platelets were pretreated with Bort or its Veh and subsequently stimulated with increasing concentrations of U46619, ADP, or thrombin as described in the Methods section. After 15 minutes, PAC-1 binding was assessed by flow cytometry. The bars represent the mean±SEM of 3 independent experiments.

Supplemental Figure 4. *MG132 attenuates proplatelet formation*. Human megakaryocytes were left alone (NT – no treatment) or treated with MG132 and then analyzed by confocal microscopy (6 hours post-MG132). The images show megakaryocytes stained with WGA (red) and phalloidin (green) where white arrows point to proplatelet extensions and yellow arrows point to non-proplatelet producing megakaryocytes. Scale bar = 50μm. The bar graph on the right depicts the relative change in proplatelet producing megakaryocytes in MG132 treated

cells compared to untreated cells. The bars represent the mean±SEM of 3 independent experiments and the asterisk is $p<0.05$ compared to NT.

Supplemental Figure 5. *Inhibition of the proteasome does not alter $\alpha_{IIb}\beta_3$ activity in human megakaryocytes*. (**A**) $CD34^+$-derived human megakaryocytes were treated with Veh or Bort and binding of soluble fibrinogen (FGN), in the presence or absence of 0.05 U/ml of thrombin (Thr), was assessed as described in the Methods section. The bars represent the mean±SEM of 3 experiments and the asterisk identifies $p<0.05$ when comparing megakaryocytes with and without Thr to one another. There was no difference in soluble FGN binding when comparing Veh to Bort treated megakaryocytes. MFI = mean fluorescent intensity. (**B**) PAC-1 binding to megakaryocytes in the presence of Bort, Veh, or Thr (0.05 U/ml). The bars represent the mean±SEM of 3 experiments and the asterisk identifies $p<0.05$ compared to Thr-treated megakaryocytes.

Supplemental Figure 6. *Inhibition of the proteasome does not alter adherence of human megakaryocytes to fibrinogen*. Human megakaryocytes were placed on immobilized fibrinogen for 1 hour in the presence of Veh or Bort. The cells were analyzed by confocal microscopy and adhered megakaryocytes were counted in five different fields. The bars represent the mean±SEM of 2 independent experiments.

Supplemental Figure 7. *The proteasome regulates human proplatelet formation through the RhoA signaling pathway*. Human megakaryocytes were treated with Veh, Bort, or Bort + C3 transferase and the change in the relative number of proplatelet producing megakaryocytes in treated groups compared to Veh was assessed. The bars in this figure represent the mean±SEM of 3 independent experiments. The asterisk is $p<0.05$ compared to Veh.

Supplemental Figure 8. *Psmc1 protein is expressed in human and mouse megakaryocytes*. Human $CD34^{+}$-derived and mouse bone marrow derived proplatelet producing megakaryocytes lysates were separated by SDS-Page and protein for Psmc1 was assessed. Lanes 1 and 2 show Psmc1 protein expression levels in two independent human megakaryocyte samples. Lanes 3 and 4 show Psmc1 protein expression in two independent mouse megakaryocyte samples.

Supplemental Figure 9. *Protein for Psmc1 is reduced in megakaryocytes, but not other tissues, isolated from* $Psmc1^{fl/fl}$*;PF4cre.* (**A**) Western blot of megakaryocyte lysates obtained from $Psmc1^{fl/wt}$ and $Psmc1^{fl/fl}$*;PF4cre* mice. Protein for Psmc1 is shown in the top panel. After Psmc1 protein levels were assessed, the gel was stained with coomassie blue. A coomassie stained region of this gel is shown in the bottom panel. This image is representative of 4 independent experiments. (**B**) Western blot of Psmc1 protein expression in megakaryocytes, brain, heart, liver and thymus from $Psmc1^{fl/wt}$ and $Psmc1^{fl/fl}$*;PF4cre* mice. After Psmc1 protein levels were assessed, the gel was stained with coomassie blue. Coomassie stained regions for each tissue are shown in the bottom panel.

Supplemental Figure 10. *Genetic ablation of proteasome activity in megakaryocytes increases protein ubiquitination.* The top left panel shows a representative western blot of ubiquitinated proteins in megakaryocytes derived from $Psmc1^{fl/wt}$ and $Psmc1^{fl/fl}$*;Pf4cre* mice. The corresponding coomassie image of this gel is shown directly below. The bars in the right panel show the relative change in ubiquitin expression in megakaryocytes from $Psmc1^{fl/fl}$*;PF4cre* mice compared to $Psmc1^{fl/wt}$ mice. The asterisk is $p<0.05$ compared to $Psmc1^{fl/wt}$ mice.

Supplemental Figure 11. *Deletion of Psmc1 in megakaryocytes does not alter the number of megakaryocytes found in the bone marrow or spleen.* Sections of bone marrow and spleen were stained for von Willebrand Factor (vWF) and vWF positive megakaryocytes were assessed in *Psmc1$^{fl/wt}$* and *Psmc1$^{fl/fl}$;PF4cre* mice. The left panels show representative bone marrow and spleen tissue sections. Higher magnification insets from the spleen tissue sections are shown at the very bottom. The red boxes indicate the region of the spleen selected for the inset. Scale bars for full images = 50μm. Scale bars for insets = 20μm. In the far right panel, the number of megakaryocytes in the bone marrow and spleen were counted as described in the Methods section. The bars on the right represent the mean±SEM of tissue sections from 3 *Psmc1$^{fl/wt}$* and 3 *Psmc1$^{fl/fl}$;PF4cre* mice.

Supplemental Figure 12. *c-mpl and Psmc1$^{fl/fl}$;PF4cre mice are thrombocytopenic, but platelet counts are lower in Psmc1$^{fl/fl}$;PF4cre mice.* Platelet counts at P3 in *Psmc1$^{fl/wt}$* and *Psmc1$^{fl/fl}$;PF4cre* mice were compared to platelet counts from *c-mpl* knockout mice (*c-mpl$^{ko/ko}$*) and their littermate controls (*c-mpl$^{wt/wt}$*). As shown in this figure, thrombocytopenia is observed in both the *c-mpl$^{ko/ko}$* and *Psmc1$^{fl/fl}$;PF4cre* mice but is more severe in the *Psmc1$^{fl/fl}$;PF4cre* mice. The bars represent the mean±SEM of platelet counts obtained from 6 mice for each experimental group. The asterisk is $p<0.05$ between groups designated by the lines above the bars.

Supplemental Figure 13. *Inducible deletion of Psmc1 in Pdgfcre-ER mice at P1 results in thrombocytopenia and death*. (**A**) Relative changes in platelet counts in *Psmc1$^{fl/fl}$;Pdgf-creER* mice compared to *Psmc1$^{fl/fl}$ and Psmc1$^{fl/wt}$* mice. Platelet counts were determined 1 day post-tamoxifen. The bars represent the mean±SEM of 3 independent experiments and the asterisk is $p<0.05$ compared to control mice. (**B**) Mortality rates in *Psmc1$^{fl/fl}$ and Psmc1$^{fl/wt}$* compared to

Psmc1$^{fl/fl}$*;Pdgf-creER* mice treated with tamoxifen on postnatal day 1 (P1). Mortality was assessed at postnatal day 2 (P2) and 21 (P21). The bars represent a Chi-square analysis comparing the expected versus observed genotypes at P1 and P21 (n=82) where the asterisk denotes significance as determined by a Chi-square distribution table.

Supplemental Figure 14. *Bortezomib blunts human platelet aggregation in response to low dose thrombin*. Washed human platelets were preincubated with Veh or Bort and stimulated with low dose (0.05 U/ml) thrombin in the left panel or high dose (0.2 U/ml) thrombin in the right panel. Aggregation was monitored by light transmittance using a Chronolog platelet aggregometer. The platelet aggregation tracings are representative of three independent experiments.

Supplemental Table 1. *Expression of transcripts coding for proteasome subunits in human and mouse megakaryocytes***.** Poly-A RNA isolated from CD34^{+}-derived human megakaryocytes and fetal liver derived mouse megakaryocytes were sequenced on an Illumina genome analyzer. Reads were aligned and RPKM (reads per kilobase per million) expression estimates were calculated as previously described (45). RPKM values with a threshold at $\leq$0.3 identify mRNAs with expression levels above background (45, 52). Transcripts listed are proteasome subunits found within the gene ontology term “proteasome complex.”

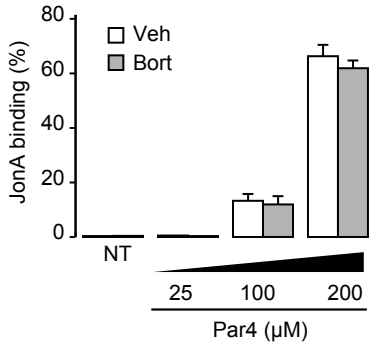

Supplemental Figure 1
D Shi & M Smith, et al.

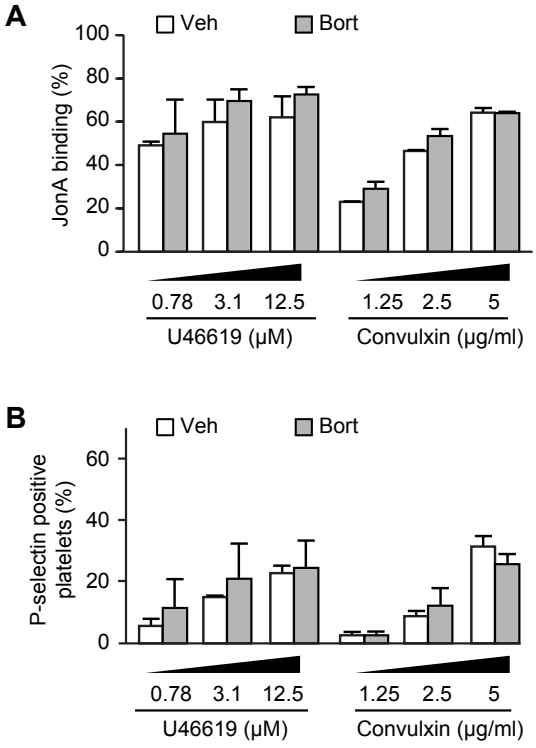

Supplemental Figure 2
D Shi & M Smith, et al.

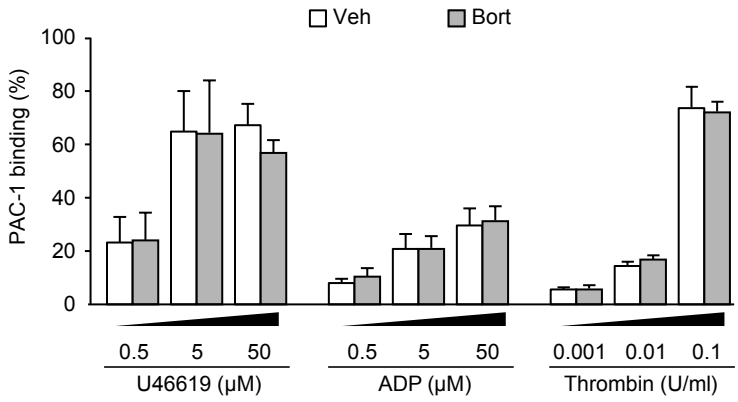

Supplemental Figure 3
D Shi & M Smith, et al.

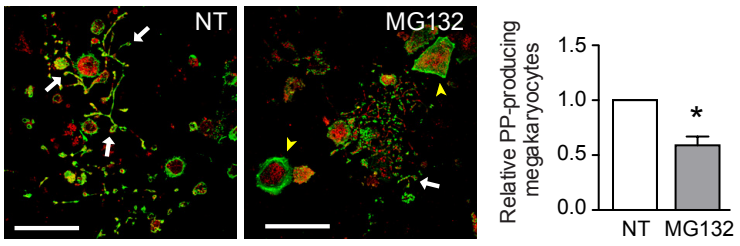

Supplemental Figure 4
D Shi & M Smith, et al.

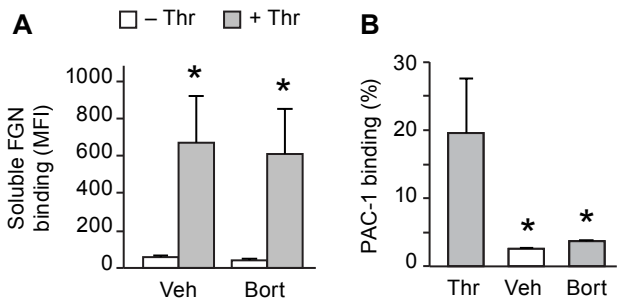

Supplemental Figure 5
D Shi & M Smith, et al.

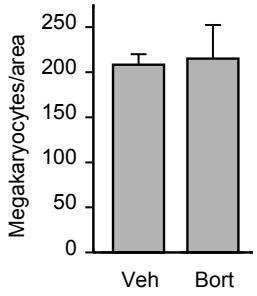

Supplemental Figure 6
D Shi & M Smith, et al.

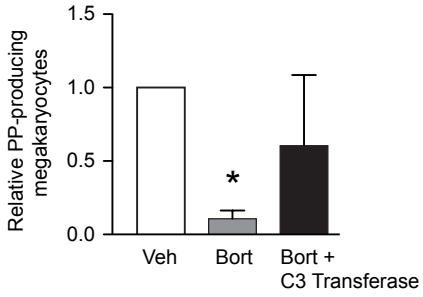

Supplemental Figure 7
D Shi & M Smith, et al.

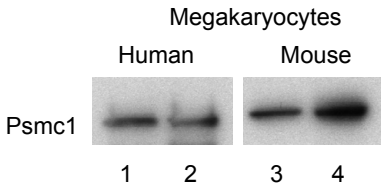

Supplemental Figure 8
D Shi & M Smith, et al.

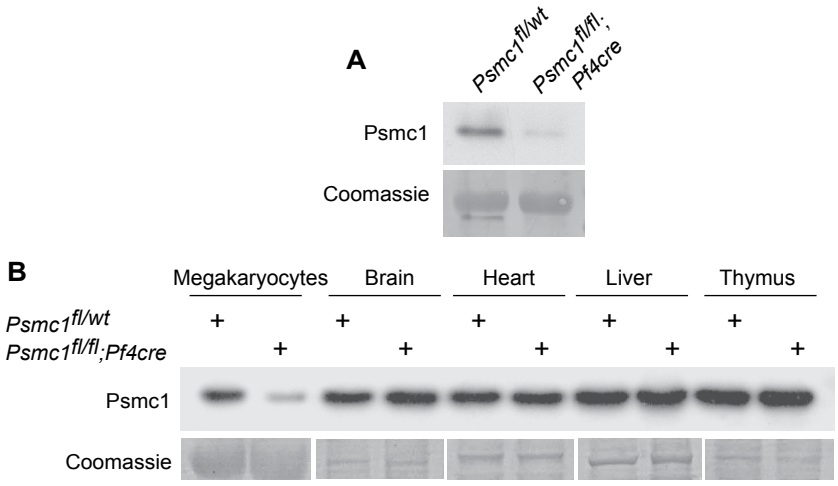

Supplemental Figure 9
D Shi & M Smith, et al.

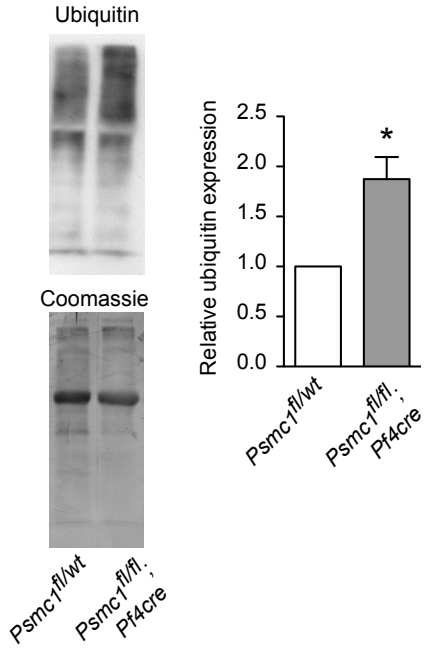

Supplemental Figure 10
D Shi & M Smith, et al.

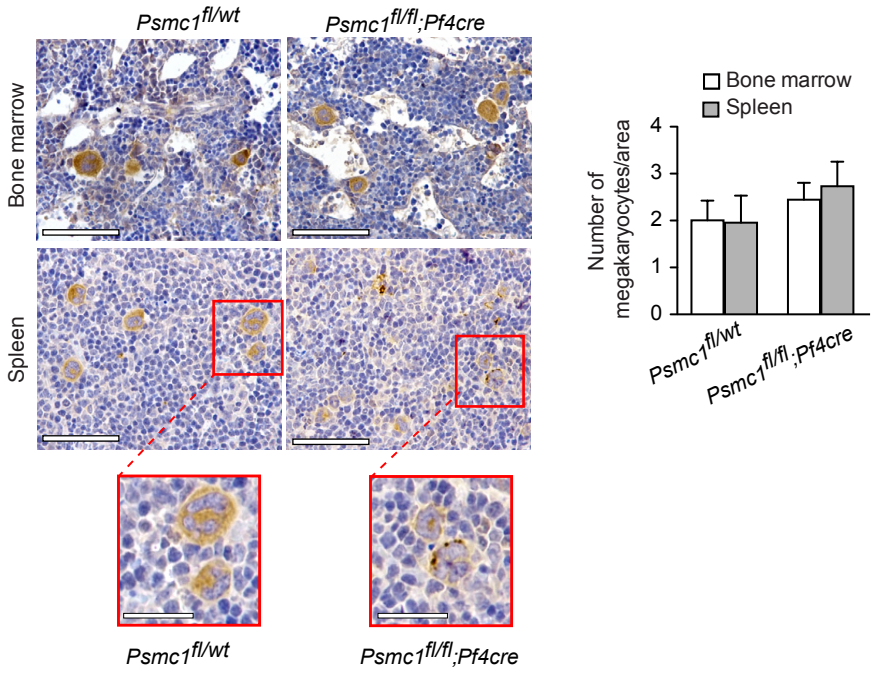

Supplemental Figure 11
D Shi & M Smith, et al.

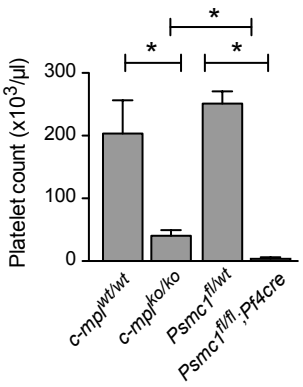

Supplemental Figure 12
D Shi & M Smith, et al.

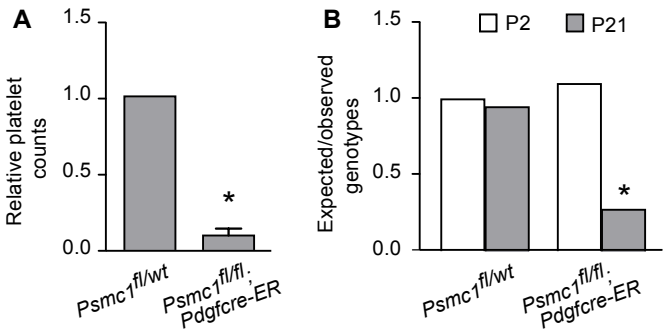

Supplemental Figure 13
D Shi & M Smith, et al.

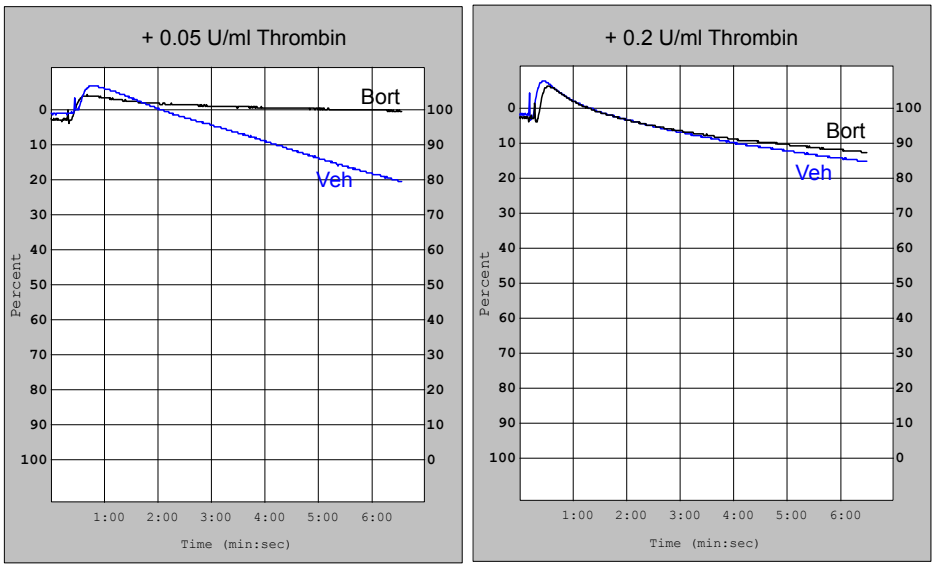

Supplemental Figure 14
D Shi & M Smith, et al.

Supplemental Table 1.

Gene	Human $CD34^+$ Megs	Murine Fetal Liver Megs
proteasome 26S subunit, ATPase, 1	2.07	38.73
proteasome 26S subunit, ATPase, 2	30.23	16.62
proteasome 26S subunit, ATPase, 3	112.71	44.12
proteasome 26S subunit, ATPase, 4	90.42	26.15
proteasome 26S subunit, ATPase, 5	143.93	41.51
proteasome 26S subunit, ATPase, 6	13.60	40.92
proteasome 26S subunit, non-ATPase, 1	58.30	25.59
proteasome 26S subunit, non-ATPase, 2	95.75	43.05
proteasome 26S subunit, non-ATPase, 3	113.65	15.10
proteasome 26S subunit, non-ATPase, 4	67.07	85.09
proteasome 26S subunit, non-ATPase, 5	8.08	12.86
proteasome 26S subunit, non-ATPase, 6	103.13	31.87
proteasome 26S subunit, non-ATPase, 7	73.95	32.28
proteasome 26S subunit, non-ATPase, 8	115.63	128.93
proteasome 26S subunit, non-ATPase, 9	24.49	5.45
proteasome 26S subunit, non-ATPase, 10	22.52	20.26
proteasome 26S subunit, non-ATPase, 11	64.91	33.28
proteasome 26S subunit, non-ATPase, 12	25.27	22.85
proteasome 26S subunit, non-ATPase, 13	73.65	39.99
proteasome 26S subunit, non-ATPase, 14	39.55	19.04
proteasome subunit, alpha type, 1	54.43	38.70
proteasome subunit, alpha type, 2	22.37	33.71
proteasome subunit, alpha type, 3	60.60	5.50
proteasome subunit, alpha type, 4	92.04	28.32
proteasome subunit, alpha type, 5	105.97	12.41
proteasome subunit, alpha type, 6	80.73	116.02
proteasome subunit, alpha type, 7	187.17	36.16
proteasome subunit, beta type, 1	166.42	182.02
proteasome subunit, beta type, 2	71.94	47.88
proteasome subunit, beta type, 3	125.76	8.63
proteasome subunit, beta type, 4	224.93	91.72
proteasome subunit, beta type, 5	67.47	38.21
proteasome subunit, beta type, 6	114.32	38.13
proteasome subunit, beta type, 7	123.10	51.79
proteasome subunit, beta type, 10	36.24	22.47